

Sub-Doppler spectroscopy of alkali vapors confined in nanometric and micrometric thin cells

Mr. Rodolphe MOMIER

A thesis in Physics
Presented for the degree of Doctor of Philosophy

Laboratoire Interdisciplinaire Carnot de Bourgogne, UMR 6303 CNRS - Université Bourgogne Franche-Comté, Dijon,
France
and

Institute for Physical Research - NAS of Armenia, Ashtarak, Armenia

September 17th, 2024

Mr. SARGSYAN Armen

Doctor of Physics
Institute for Physical Research, Armenia

Co-supervisor

Mr. PAPOYAN Aram

Professor of Physics
Institute for Physical Research, Armenia

Supervisor

Mr. LEROY Claude

Professor of Physics
Laboratoire ICB, Université de Bourgogne, France

Supervisor

Introduction

Nanometric thin cell spectroscopy

Alkali vapors in a magnetic field

Transition cancellations

Magnetometry with thin cells

EIT resonances using “forbidden” transitions

Conclusion

Why are nanocells useful?

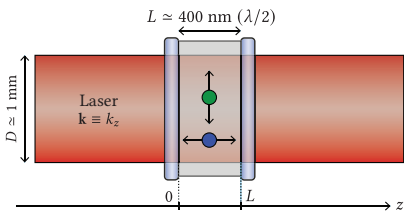


Figure: Schematic diagram of a NC of thickness L with a laser propagating along z .

Why are nanocells useful?

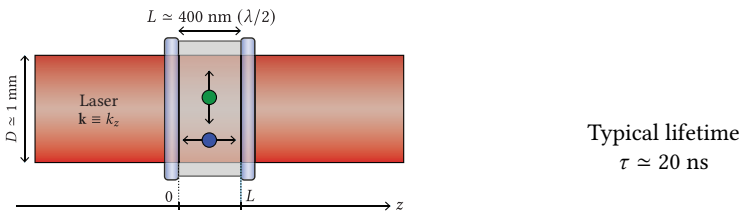


Figure: Schematic diagram of a NC of thickness L with a laser propagating along z .

Why are nanocells useful?

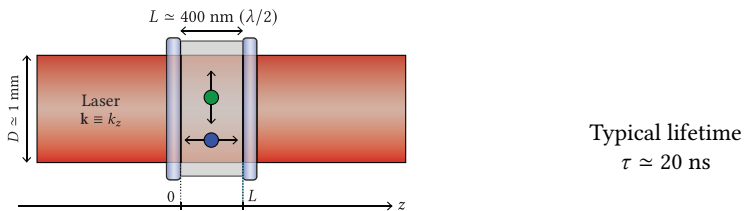


Figure: Schematic diagram of a NC of thickness L with a laser propagating along z .

Along the laser beam

$$t_L = \frac{L}{v_z} = \frac{400 \cdot 10^{-9}}{300} \approx 1.3 \text{ ns}$$

Why are nanocells useful?

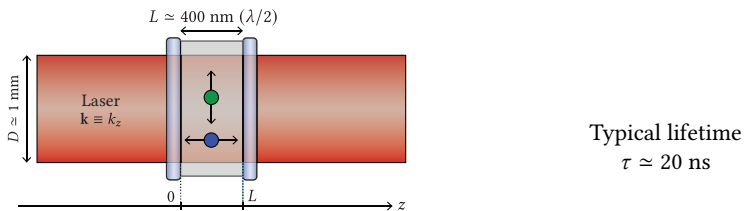


Figure: Schematic diagram of a NC of thickness L with a laser propagating along z .

Along the laser beam

$$t_L = \frac{L}{v_z} = \frac{400 \cdot 10^{-9}}{300} \simeq 1.3 \text{ ns}$$

Across the laser beam

$$t_D = \frac{D}{v_x} = \frac{10^{-3}}{300} \simeq 3 \mu\text{s}$$

Why are nanocells useful?

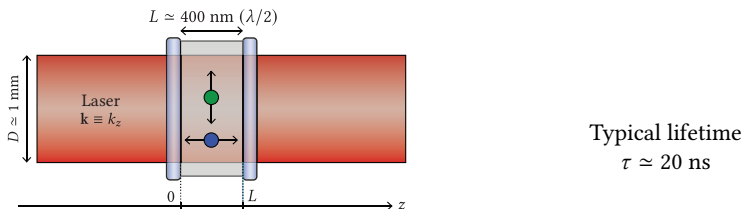


Figure: Schematic diagram of a NC of thickness L with a laser propagating along z .

Along the laser beam

$$t_L = \frac{L}{v_z} = \frac{400 \cdot 10^{-9}}{300} \approx 1.3 \text{ ns}$$

Across the laser beam

$$t_D = \frac{D}{v_x} = \frac{10^{-3}}{300} \approx 3 \mu\text{s}$$

Doppler broadening: gone!

Only have flying across the beam have time to be pumped ($t_D \gg \tau$) but for these atoms, $\mathbf{k} \cdot \mathbf{v} = 0$. The geometry of the cell itself “kills” Doppler broadening.

What is a nanocell?

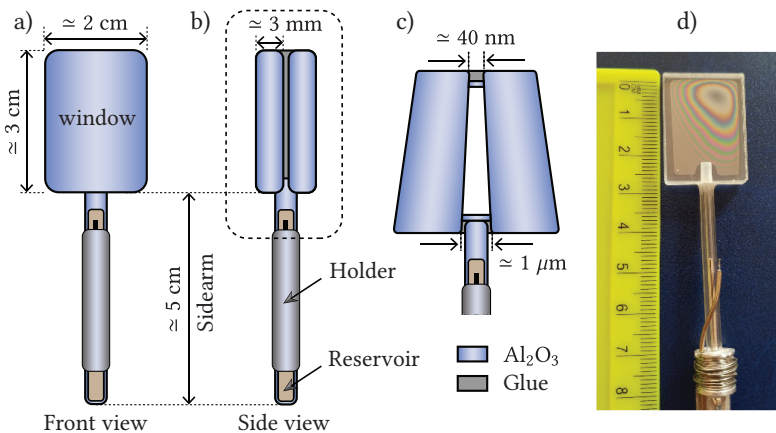


Figure: Front (a) and side (b-c) views of a NC with typical dimensions. c) Zoom on dashed rectangle showing the wedged structure of the cell. d) Photograph of a NC.

What are its advantages?

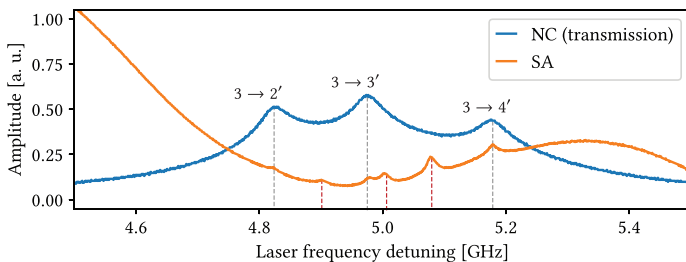


Figure: Blue: experimental transmission spectrum of the $3 \rightarrow 2', 3', 4'$ transitions of Cs D_2 line recorded with a NC ($L = \lambda/2$, $T = 110^\circ\text{C}$). Orange: SA spectrum recorded with a cm-long cell. The grey dashed lines indicate the position of the transitions and the red dashed lines indicate cross-over resonances.

- Sub-Doppler spectroscopy with a single beam/pass
 - Full resolution of hyperfine structure can be achieved: magnetometry
 - Clean absorption and reflection spectra
 - No crossover resonances
 - Correct transition strengths

Introduction

Nanometric thin cell spectroscopy

- Fabry-Pérot nanocavity model
- Theoretical results

Alkali vapors in a magnetic field

Transition cancellations

Magnetometry with thin cells

EIT resonances using “forbidden” transitions

Conclusion

FP nanocavity model: geometry of the problem

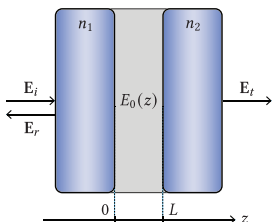
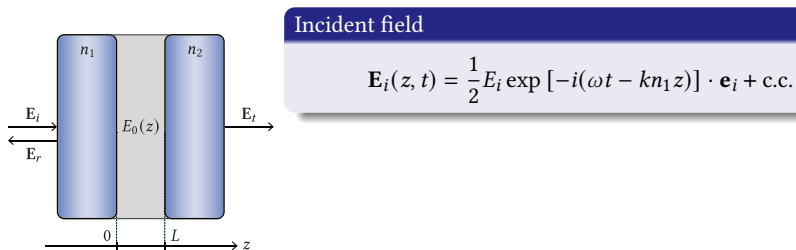


Figure: Scheme of a cavity of thickness L .

G. Dutier, S. Saltiel, D. Bloch, and M. Ducloy. Revisiting optical spectroscopy in a thin vapor cell: mixing of reflection and transmission as a Fabry-Perot microcavity effect. *J. Opt. Soc. Am. B* 20 (5) (2003), 793–800.

FP nanocavity model: geometry of the problem



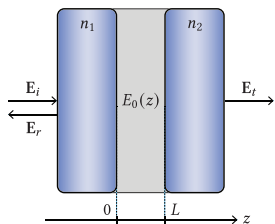
Incident field

$$\mathbf{E}_i(z, t) = \frac{1}{2} E_i \exp [-i(\omega t - kn_1 z)] \cdot \mathbf{e}_i + \text{c.c.}$$

Figure: Scheme of a cavity of thickness L .

G. Dutier, S. Saltiel, D. Bloch, and M. Ducloy. Revisiting optical spectroscopy in a thin vapor cell: mixing of reflection and transmission as a Fabry-Pérot microcavity effect. *J. Opt. Soc. Am. B* **20** (5) (2003), 793–800.

FP nanocavity model: geometry of the problem



Incident field

$$\mathbf{E}_i(z, t) = \frac{1}{2} E_i \exp [-i(\omega t - kn_1 z)] \cdot \mathbf{e}_i + \text{c.c.}$$

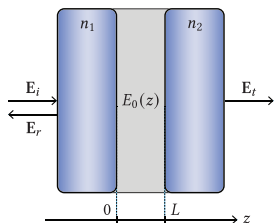
Fields inside the vapor medium

$$\mathbf{E}_0(z, t) = \frac{1}{2} E_0(z) \exp[-i(\omega t - kz)] + \text{c.c.}$$

$$\mathbf{P}_0(z, t) = \frac{1}{2} P_0(z) \exp[-i(\omega t - kz)] + \text{c.c.}$$

Figure: Scheme of a cavity of thickness L .

FP nanocavity model: geometry of the problem



Incident field

$$\mathbf{E}_i(z, t) = \frac{1}{2} E_i \exp [-i(\omega t - kn_1 z)] \cdot \mathbf{e}_i + \text{c.c.}$$

Fields inside the vapor medium

$$\mathbf{E}_0(z, t) = \frac{1}{2} E_0(z) \exp [-i(\omega t - kz)] + \text{c.c.}$$

$$\mathbf{P}_0(z, t) = \frac{1}{2} P_0(z) \exp [-i(\omega t - kz)] + \text{c.c.}$$

Figure: Scheme of a cavity of thickness L .

Goal

Express the reflected and transmitted amplitudes (E_r, E_t) and intensities (I_r, I_t)

G. Dutier, S. Saltiel, D. Bloch, and M. Ducloy. Revisiting optical spectroscopy in a thin vapor cell: mixing of reflection and transmission as a Fabry-Pérot microcavity effect. *J. Opt. Soc. Am. B* **20** (5) (2003), 793–800.

Reflected and transmitted amplitudes

Decomposition into two fields

$$|E_t|^2 = \left|E_t^{\text{FP}}\right|^2 + \left|E_t^{\text{R}}\right|^2 + 2 \operatorname{Re} [E_t^{\text{FP}} E_t^{\text{R}}]$$

$$|E_r|^2 = \left|E_r^{\text{FP}}\right|^2 + \left|E_r^{\text{R}}\right|^2 + 2 \operatorname{Re} \left[E_r^{\text{FP}} E_r^{\text{R}} \right]$$

Reflected and transmitted signals

$$S_t = 2 \frac{t_{02}^2 t_{10}}{|F|^2} \operatorname{Re} [I_f - r_1 I_b]$$

$$S_r = 2 \frac{E_1 t_{01}}{|F|^2} \operatorname{Re} \left[\{r_1 - r_2 \exp(-2ikL)\} \{I_b - r_2 \exp(2ikL) I_f\} \right]$$

Reflected and transmitted amplitudes

Decomposition into two fields

$$|E_t|^2 = \left|E_t^{\text{FP}}\right|^2 + \left|E_t^{\text{R}}\right|^2 + 2 \operatorname{Re} \left[E_t^{\text{FP}} E_t^{\text{R}} \right]$$

$$|E_r|^2 = \left|E_r^{\text{FP}}\right|^2 + \left|E_r^{\text{R}}\right|^2 + 2 \operatorname{Re} \left[E_r^{\text{FP}} E_r^{\text{R}} \right]$$

Reflected and transmitted signals

$$S_t = 2 \frac{t_{02}^2 t_{10}}{|F|^2} \operatorname{Re} [I_f - r_1 I_b]$$

$$S_r = 2 \frac{E_i t_{01}}{|F|^2} \operatorname{Re} \left[\{r_1 - r_2 \exp(-2ikL)\} \{I_b - r_2 \exp(2ikL) I_f\} \right]$$

Goal

Express the forward and backward atomic response!

Atomic response

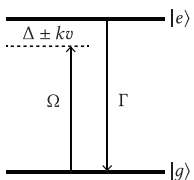
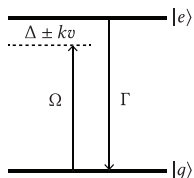


Figure: Scheme of a two-level system of decay rate Γ driven by the Rabi frequency Ω .

M. Auzinsh, D. Budker, and S. M. Rochester. *Optically Polarized Atoms : Understanding Light-Atom Interactions*. (2010).

Atomic response



Macroscopic polarization

$$P_o(z, \omega) = Nd \langle \rho_{eg}(z, v) \rangle = Nd_{eg} \int M(v) \rho_{eg}(z, v) dv$$

Figure: Scheme of a two-level system of decay rate Γ driven by the Rabi frequency Ω .

M. Auzinsh, D. Budker, and S. M. Rochester. *Optically Polarized Atoms : Understanding Light-Atom Interactions.* (2010).

Atomic response

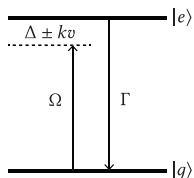


Figure: Scheme of a two-level system of decay rate Γ driven by the Rabi frequency Ω .

Macroscopic polarization

$$P_o(z, \omega) = Nd \langle \rho_{eg}(z, v) \rangle = Nd_{eg} \int M(v) \rho_{eg}(z, v) dv$$

Liouville – von Neumann equation

$$\frac{d\rho}{dt} = -\frac{i}{\hbar} [\mathcal{H}, \rho] + \mathcal{L}(\rho)$$

Atomic response

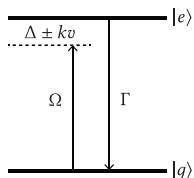


Figure: Scheme of a two-level system of decay rate Γ driven by the Rabi frequency Ω .

Macroscopic polarization

$$P_o(z, \omega) = Nd \langle \rho_{eg}(z, v) \rangle = Nd_{eg} \int M(v) \rho_{eg}(z, v) dv$$

Liouville – von Neumann equation

$$\frac{d\rho}{dt} = -\frac{i}{\hbar} [\mathcal{H}, \rho] + \mathcal{L}(\rho)$$

Coherences (steady state)

$$v \frac{\partial \sigma_{eg}}{\partial z} = i\Omega(\sigma_{gg} - \sigma_{ee}) - \Lambda_{\pm}\sigma_{eg}$$

M. Auzinsh, D. Budker, and S. M. Rochester. *Optically Polarized Atoms : Understanding Light-Atom Interactions.* (2010).

Lineshape analysis

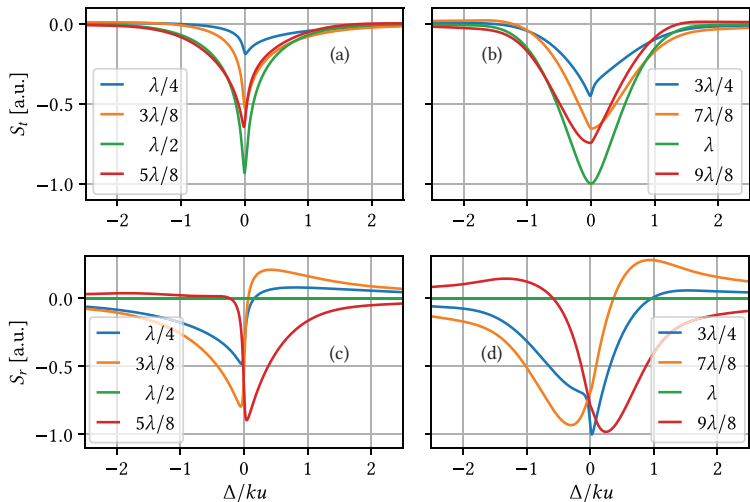


Figure: Normalized transmitted (a-b) and reflected (c-d) signals S_t and S_r for various cell thicknesses in a cell made of two identical sapphire windows. The lines were calculated with $\gamma/ku = 0.025$.

Ensemble of two – level systems

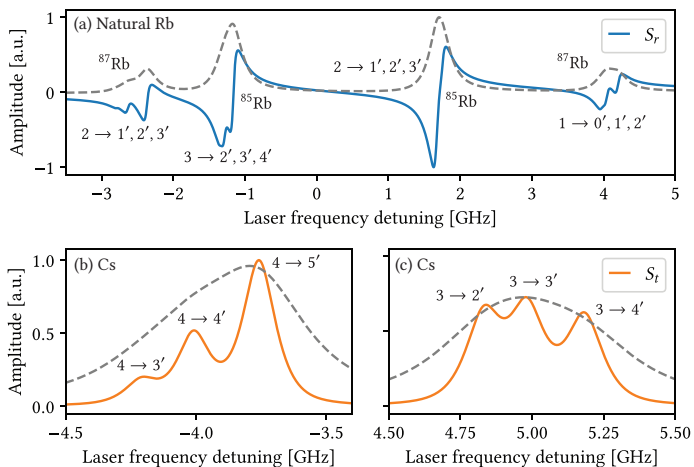


Figure: (a) Typical theoretical SR (S_r) spectrum of Cs D_2 line obtained for $L = 350$ nm. (b-c) Theoretical transmission spectrum of Cs D_2 line obtained for $L = \lambda/2$. The dashed lines are usual Doppler-broadened transmission profiles that would be obtained in regular cells.

Comparison with experimental measurements

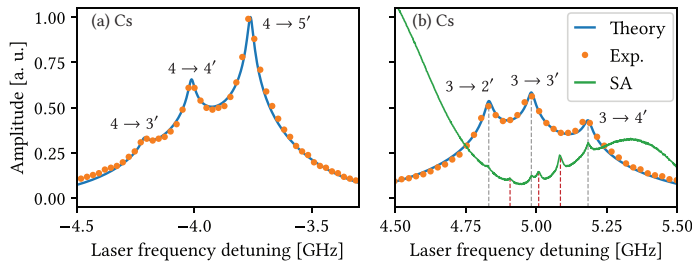


Figure: Theoretical (blue) and experimental (orange dots) spectra of Cs D_2 line $4 \rightarrow 3'$, $4'$, $5'$ transitions (a) and $3 \rightarrow 2'$, $3'$, $4'$ transitions (b) recorded with a NC ($L = \lambda/2$, $T = 110^\circ\text{C}$). Green: SA spectrum recorded with a usual cm-long cell. The grey dashed lines indicate the position of the transitions and the red dashed lines indicate cross-over resonances.

Conclusion

Excellent agreement between theory and experiment. NC spectra are much cleaner than usual SA spectra obtained in long cells.

Alkali vapors in a magnetic field

- Theoretical model
 - Spectra of Sodium D_2 line
 - Magnetically-Induced Circular Dichroism

Magnetometry with thin cells

Conclusion

Theory - Magnetic Hamiltonian

The magnetic Hamiltonian including nuclear spin (from Dirac equation) reads

$$\mathcal{H}_m = \frac{\mu_B}{\hbar} B_z (g_L L_z + g_S S_z + g_I I_z) .$$

Theory - Magnetic Hamiltonian

The magnetic Hamiltonian including nuclear spin (from Dirac equation) reads

$$\mathcal{H}_m = \frac{\mu_B}{\hbar} B_z (g_L L_z + g_S S_z + g_I I_z) .$$

The matrix elements of \mathcal{H} are:

$$\langle F, m_F | \mathcal{H} | F, m_F \rangle = E_0(F) - \mu_B g_F m_F B_z$$

P. Tremblay, A. Michaud, M. Levesque, S. Thériault, M. Breton, J. Beaubien, and N. Cyr. *Absorption profiles of alkali-metal D lines in the presence of a static magnetic field*. Phys. Rev. A. 42 (1990), 2766–2773.

Theory - Magnetic Hamiltonian

The magnetic Hamiltonian including nuclear spin (from Dirac equation) reads

$$\mathcal{H}_m = \frac{\mu_B}{\hbar} B_z (g_L L_z + g_S S_z + g_I I_z).$$

The matrix elements of \mathcal{H} are:

$$\langle F, m_F | \mathcal{H} | F, m_F \rangle = E_0(F) - \mu_B g_F m_F B_z$$

$$\begin{aligned} \langle F-1, m_F | \mathcal{H} | F, m_F \rangle = & -\frac{\mu_B}{2} (g_J - g_I) B_z \left(\frac{[(J+I+1)^2 - F^2][F^2 - (J-I)^2]}{F} \right)^{1/2} \\ & \times \left(\frac{F^2 - m_F^2}{F(2F+1)(2F-1)} \right)^{1/2}. \end{aligned}$$

With $|J - I| \leq F \leq J + I$ and $-F \leq m_F \leq F$.

P. Tremblay, A. Michaud, M. Levesque, S. Thériault, M. Breton, J. Beaubien, and N. Cyr. *Absorption profiles of alkali-metal D lines in the presence of a static magnetic field*. Phys. Rev. A. 42 (1990), 2766–2773.

Theory - Magnetic Hamiltonian

Remark

The Hamiltonian is m_F -block diagonal. The off-diagonal elements obey $\Delta F = \pm 1$, $\Delta m_F = 0$.

Theory - Magnetic Hamiltonian

Remark

The Hamiltonian is m_F -block diagonal. The off-diagonal elements obey $\Delta F = \pm 1$, $\Delta m_F = 0$.

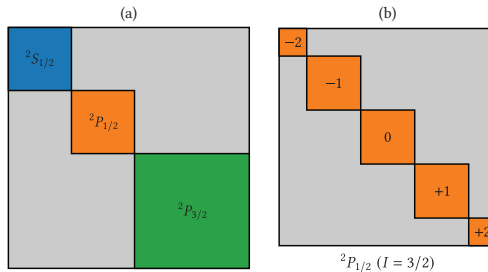


Figure: Block structure of the magnetic Hamiltonian. a) Blocks representing the fine states. b) close-up on the $^2P_{1/2}$ state: the matrix is block diagonal in the $|F, m_F\rangle$ basis, each block corresponding to a different value of m_F , and F is equal to either 1 or 2.

Theory - Transfer coefficients

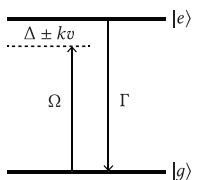
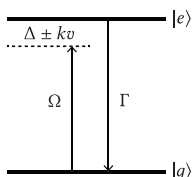


Figure: Two-level system (two Zeeman states) of resonant frequency ν and lifetime $1/\Gamma_e$.

P. Tremblay, A. Michaud, M. Levesque, S. Thériault, M. Breton, J. Beaubien, and N. Cyr. *Absorption profiles of alkali-metal D lines in the presence of a static magnetic field*. Phys. Rev. A. 42 (1990), 2766–2773.

E. De Clercq, M. De Labachellerie, G. Avila, P. Cerez, and M. Tetu. *Laser diode optically pumped caesium beam*. J. de Physique 45 (2) (1984), pp. 239–247.

Theory - Transfer coefficients



The matrix elements of the electric dipole components are

$$|\langle e | D_q | g \rangle|^2 = \frac{3\epsilon_0 \hbar \lambda^3}{8\pi^2} A_{eg},$$

Figure: Two-level system (two Zeeman states) of resonant frequency ν and lifetime $1/\Gamma_e$.

P. Tremblay, A. Michaud, M. Levesque, S. Thériault, M. Breton, J. Beaubien, and N. Cyr. *Absorption profiles of alkali-metal D lines in the presence of a static magnetic field*. Phys. Rev. A. 42 (1990), 2766–2773.

E. De Clercq, M. De Labachellerie, G. Avila, P. Cerez, and M. Tetu. *Laser diode optically pumped caesium beam*. J. de Physique 45 (2) (1984), pp. 239–247.

Theory - Transfer coefficients

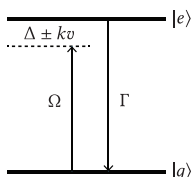


Figure: Two-level system (two Zeeman states) of resonant frequency v and lifetime $1/\Gamma_e$.

The matrix elements of the electric dipole components are

$$|\langle e | D_q | g \rangle|^2 = \frac{3\epsilon_0 \hbar \lambda^3}{8\pi^2} A_{eg},$$

where the spontaneous emission rate is

$$A_{eg} = \Gamma a^2 [\psi(F_e, m_e); \psi(F_g, m_g); q].$$

P. Tremblay, A. Michaud, M. Levesque, S. Thériault, M. Breton, J. Beaubien, and N. Cyr. *Absorption profiles of alkali-metal D lines in the presence of a static magnetic field*. Phys. Rev. A. 42 (1990), 2766–2773.

E. De Clercq, M. De Labachellerie, G. Avila, P. Cerez, and M. Tetu. *Laser diode optically pumped caesium beam*. J. de Physique 45 (2) (1984), pp. 239–247.

Theory - Transfer coefficients

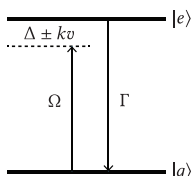


Figure: Two-level system (two Zeeman states) of resonant frequency ν and lifetime $1/\Gamma_e$.

The matrix elements of the electric dipole components are

$$|\langle e | D_q | g \rangle|^2 = \frac{3\epsilon_0 \hbar \lambda^3}{8\pi^2} A_{eg},$$

where the spontaneous emission rate is

$$A_{eg} = \Gamma a^2 [\psi(F_e, m_e); \psi(F_g, m_g); q].$$

Goal

Calculate the spontaneous emission rate.

P. Tremblay, A. Michaud, M. Levesque, S. Thériault, M. Breton, J. Beaubien, and N. Cyr. *Absorption profiles of alkali-metal D lines in the presence of a static magnetic field*. Phys. Rev. A. 42 (1990), 2766–2773.

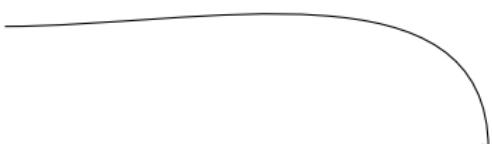
E. De Clercq, M. De Labachellerie, G. Avila, P. Cerez, and M. Tetu. *Laser diode optically pumped caesium beam*. J. de Physique 45 (2) (1984), pp. 239–247.

Theory - Transfer coefficients

The eigenvectors (mixed states) \mathcal{H}_m in the original basis of non-mixed states are:

$$|\psi(F, m)\rangle = \sum_{F'} \alpha_{F,F'} |F', m\rangle .$$

- Ground state mixing coefficients

$$a[\psi(F'_e, m_e); \psi(F'_g, m_g); q] = \sum_{F_e} \sum_{F_g} \alpha_{F_e, F'_e} a(F_e, m_e; F_g, m_g; q) \alpha_{F_g, F'_g}$$


Theory - Transfer coefficients

The eigenvectors (mixed states) \mathcal{H}_m in the original basis of non-mixed states are:

$$|\psi(F, m)\rangle = \sum_{F'} \alpha_{F,F'} |F', m\rangle .$$

- Ground state mixing coefficients
- Excited state mixing coefficients

$$a[\psi(F'_e, m_e); \psi(F'_g, m_g); q] = \sum_{F_e} \sum_{F_g} \alpha_{F_e, F'_e} \quad a(F_e, m_e; F_g, m_g; q) \quad \alpha_{F_g, F'_g}$$

Theory - Transfer coefficients

The eigenvectors (mixed states) \mathcal{H}_m in the original basis of non-mixed states are:

$$|\psi(F, m)\rangle = \sum_{F'} \alpha_{F,F'} |F', m\rangle .$$

- Ground state mixing coefficients
- Excited state mixing coefficients

$$a[\psi(F'_e, m_e); \psi(F'_g, m_g); q] = \sum_{F_e} \sum_{F_g} \alpha_{F_e, F'_e} a(F_e, m_e; F_g, m_g; q) \alpha_{F_g, F'_g}$$

- Unperturbed transfer coefficients (initial basis)

$$\begin{aligned}
 a(F_e, m_e; F_g, m_g; q) &= (-1)^{1+I+\mathcal{J}_e+F_e+F_g-m_e} \sqrt{2\mathcal{J}_e+1} \sqrt{2F_e+1} \sqrt{2F_g+1} \\
 &\times \begin{pmatrix} F_e & 1 & F_g \\ -m_e & q & m_g \end{pmatrix} \begin{Bmatrix} F_e & 1 & F_g \\ \mathcal{J}_g & I & \mathcal{J}_e \end{Bmatrix}
 \end{aligned}$$

Computational procedure

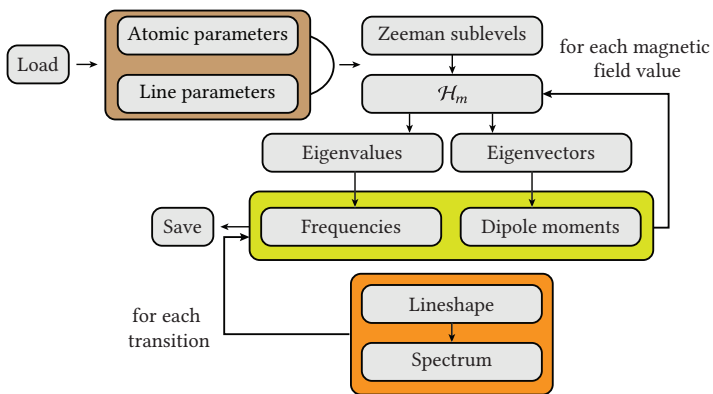


Figure: Block scheme of the program used to compute transition dipole moments, frequencies, and spectra.

Sodium D_2 line: transition intensities

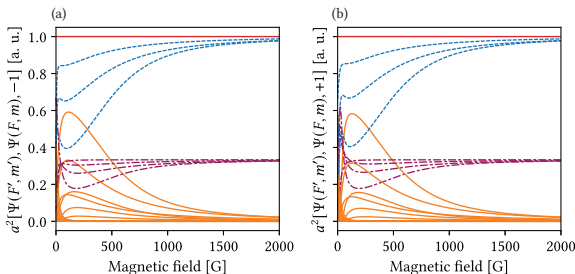


Figure: Sodium D_2 line Zeeman transition intensities. a) σ^- transitions. b) σ^+ transitions. Both panels have the same y-axis scale.

MI transitions

Forbidden transition experiencing a huge increase in intensity as B increases are called MI transitions.

Sodium D_2 line: transition intensities

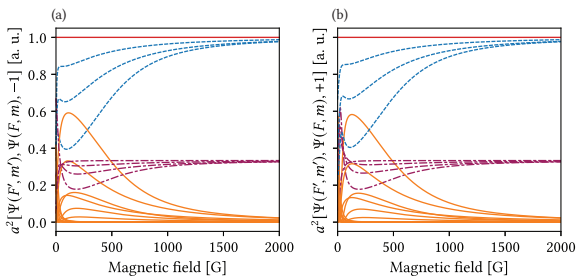


Figure: Sodium D_2 line Zeeman transition intensities. a) σ^- transitions. b) σ^+ transitions. Both panels have the same y-axis scale.

1st group (blue)

Intensity → 1

Sodium D_2 line: transition intensities

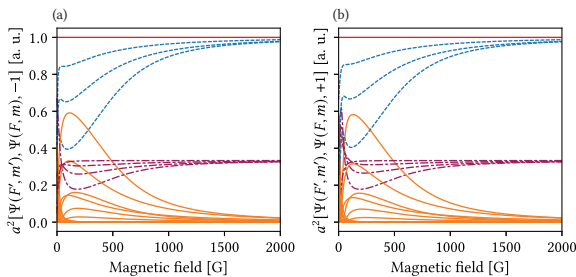


Figure: Sodium D_2 line Zeeman transition intensities. a) σ^- transitions. b) σ^+ transitions. Both panels have the same y-axis scale.

1st group (blue)

Intensity → 1

2nd group (purple)

Intensity → 0.33

Sodium D_2 line: transition intensities

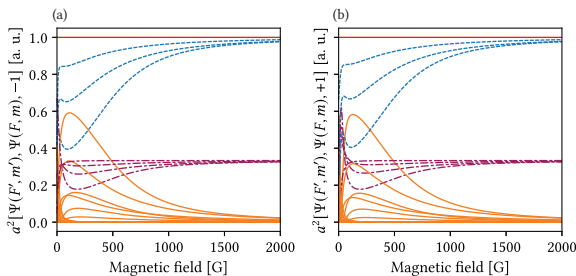


Figure: Sodium D_2 line Zeeman transition intensities. a) σ^- transitions. b) σ^+ transitions. Both panels have the same y-axis scale.

1st group (blue)

Intensity → 1

2nd group (purple)

Intensity → 0.33

3rd group (orange)

Intensity → 0

Theoretical study: Sodium D_2 line, circular polarization

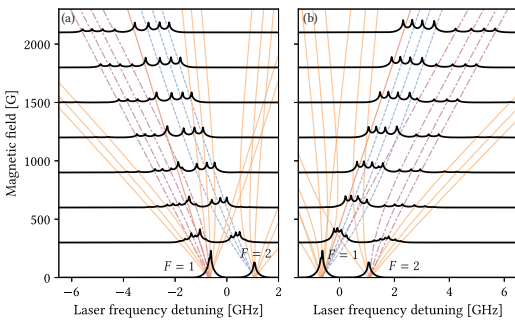


Figure: Absorption spectra of the D_2 line of sodium for a) σ^- -polarized incident laser radiation and b) σ^+ -polarized incident laser radiation. The magnetic field varies from 0 to 2100 G with a step of 300 G.

Theoretical study: Sodium D_2 line, circular polarization

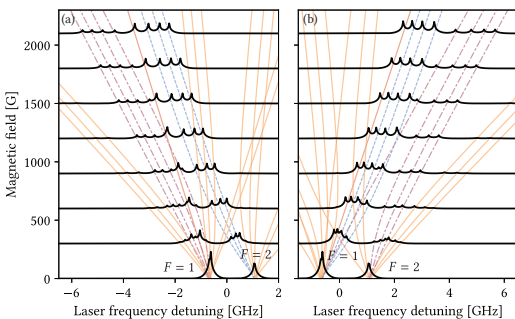


Figure: Absorption spectra of the D_2 line of sodium for a) σ^- -polarized incident laser radiation and b) σ^+ -polarized incident laser radiation. The magnetic field varies from 0 to 2100 G with a step of 300 G.

1st group (blue)

$$S \approx \mu_B$$

Theoretical study: Sodium D_2 line, circular polarization

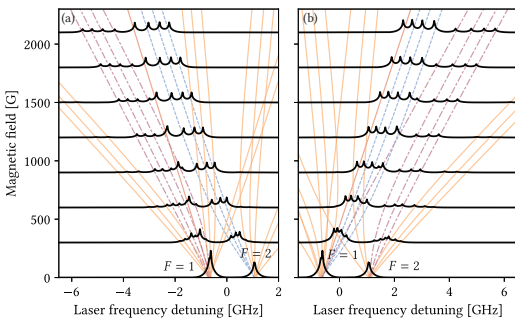


Figure: Absorption spectra of the D_2 line of sodium for a) σ^- -polarized incident laser radiation and b) σ^+ -polarized incident laser radiation. The magnetic field varies from 0 to 2100 G with a step of 300 G.

1st group (blue)

$$s \approx \mu_B$$

2nd group (purple)

$$s \simeq 5\mu_B/3$$

Theoretical study: Sodium D_2 line, circular polarization

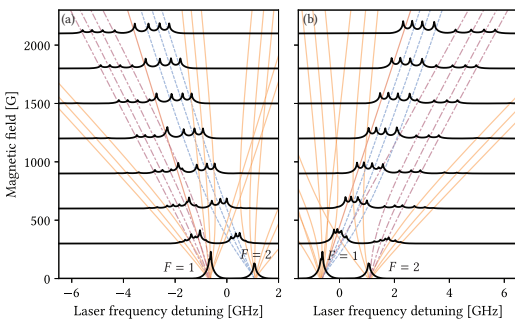


Figure: Absorption spectra of the D_2 line of sodium for a) σ^- -polarized incident laser radiation and b) σ^+ -polarized incident laser radiation. The magnetic field varies from 0 to 2100 G with a step of 300 G.

1st group (blue)

$$s \approx \mu_B$$

2nd group (purple)

$$s \simeq 5\mu_B/3$$

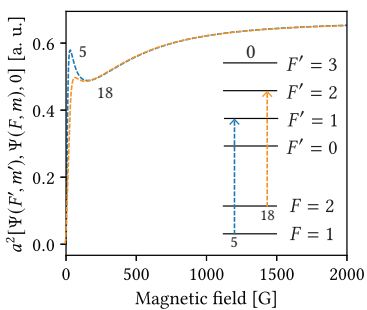
3rd group (orange)

$$s \approx 3\mu_B$$

D_2 line Circular Dichroism

1st type (MI1)

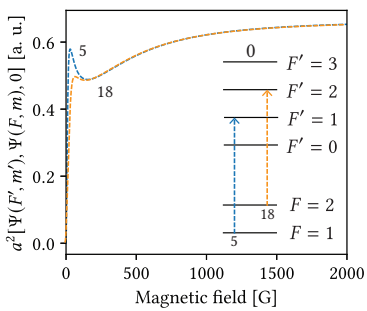
- $|F, 0\rangle \rightarrow |F' = F, 0\rangle$
- Zero probability at $B_z = 0$
- Huge increase \rightarrow max



*D*₂ line Circular Dichroism

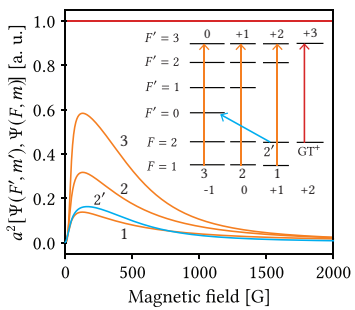
1st type (MI1)

- $|F, 0\rangle \rightarrow |F' = F, 0\rangle$
 - Zero probability at $B_z = 0$
 - Huge increase \rightarrow max



2nd type (MI2)

- $|F, m\rangle \rightarrow |F' = F \pm 2, m' - m = 0, \pm 1\rangle$
 - Steep rise
 - Probability falls back to 0



Intensity ratios

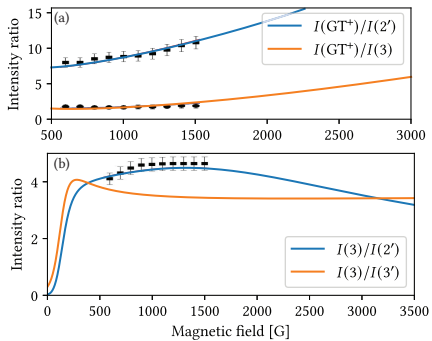


Figure: Calculated transition intensity ratios with respect to the magnetic field B_z . a) Blue curve: $I(\text{GT}^+)/I(2')$ ($|2, 1\rangle \rightarrow |0', 0'\rangle$). Orange curve: $I(\text{GT}^+)/I(3)$ ($|1, -1\rangle \rightarrow |3', 0'\rangle$) b) Blue curve: $I(3)/I(2')$. Orange curve: $I(3)/I(3')$.

Alkali vapors in a magnetic field

Transition cancellations

- Theoretical considerations
 - Analytical treatment
 - Results and experimental feasibility

Magnetometry with thin cells

Conclusion

Theoretical considerations

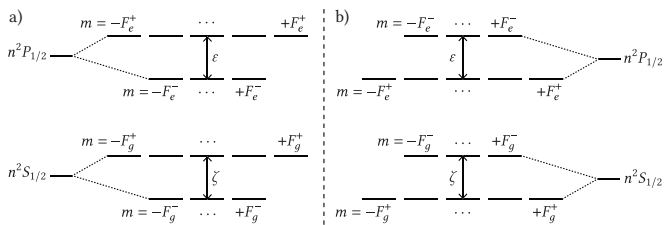


Figure: Scheme of all the possible alkali D_1 lines in a magnetic field. a) I is an integer. b) I is a half-integer (the hyperfine structure is inverted).

Theoretical considerations

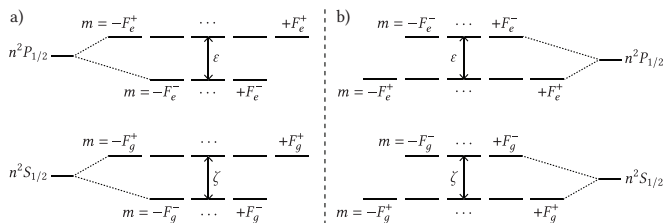


Figure: Scheme of all the possible alkali D₁ lines in a magnetic field. a) I is an integer. b) I is a half-integer (the hyperfine structure is inverted).

$$\mathcal{H}_g = \begin{bmatrix} |F_g^+, m_g\rangle & |F_g^-, m_g\rangle \\ \langle F_g^+, m_g| & \langle F_g^-, m_g| \end{bmatrix} \begin{bmatrix} \zeta - \mu_B \frac{f_g}{1+2I} m_g B & \mu_B \frac{g_g B}{2} \sqrt{1 - \left(\frac{2m_g}{1+2I}\right)^2} \\ \mu_B \frac{g_g B}{2} \sqrt{1 - \left(\frac{2m_g}{1+2I}\right)^2} & -\mu_B \left(g_I + \frac{g_g}{1+2I}\right) m_g B \end{bmatrix} \quad \begin{aligned} f_g &= g_S + 2g_I I \\ g_g &= g_I - g_S \end{aligned}$$

Theoretical considerations

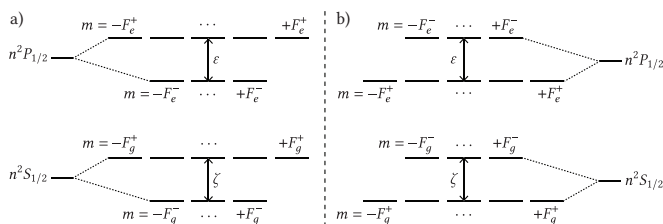


Figure: Scheme of all the possible alkali D_1 lines in a magnetic field. a) I is an integer. b) I is a half-integer (the hyperfine structure is inverted).

$$\mathcal{H}_e = \begin{bmatrix} |F_e^+, m_e\rangle \\ |F_e^-, m_e\rangle \end{bmatrix} \begin{bmatrix} \epsilon - \mu_B \frac{f_e}{1+2I} m_e B & \mu_B \frac{g_e B}{2} \sqrt{1 - \left(\frac{2m_e}{1+2I}\right)^2} \\ \mu_B \frac{g_e B}{2} \sqrt{1 - \left(\frac{2m_e}{1+2I}\right)^2} & -\mu_B \left(g_I + \frac{g_e}{1+2I}\right) m_g B \end{bmatrix} \begin{array}{l} f_e = \frac{4g_L - g_S + 6g_I I}{3} \\ g_e = \frac{3g_I - 4g_L + g_S}{3} \end{array}$$

Theoretical considerations

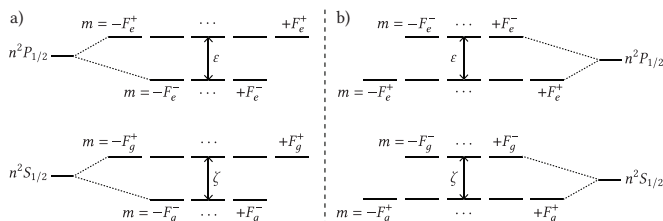


Figure: Scheme of all the possible alkali D_1 lines in a magnetic field. a) I is an integer. b) I is a half-integer (the hyperfine structure is inverted).

Eigenvalues

$$\Lambda_g^\pm = \frac{\zeta - 2\mu_B g_I m_g B}{2} \pm \frac{1}{2} \sqrt{\zeta^2 + \mu_B^2 g_g^2 B^2 + \frac{4\zeta\mu_B g_g m_g B}{2I+1}}$$

$$\Lambda_e^\pm = \frac{\epsilon - 2\mu_B g_I m_e B}{2} \pm \frac{1}{2} \sqrt{\epsilon^2 + \mu_B^2 g_e^2 B^2 + \frac{4\epsilon\mu_B g_e m_e B}{2I+1}}.$$

Theoretical considerations

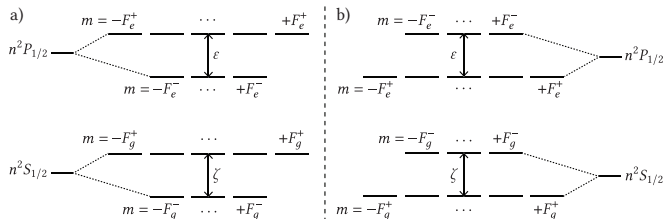


Figure: Scheme of all the possible alkali \$D_1\$ lines in a magnetic field. a) \$I\$ is an integer. b) \$I\$ is a half-integer (the hyperfine structure is inverted).

Eigenvectors

$$|\Psi(F_g^\pm, m_g)\rangle = \frac{1}{\sqrt{1 + \kappa_{g\pm}^2}} |F_g^+, m_g\rangle + \frac{\kappa_{g\pm}}{\sqrt{1 + \kappa_{g\pm}^2}} |F_g^-, m_g\rangle$$

$$|\Psi(F_e^\pm, m_e)\rangle = \frac{1}{\sqrt{1 + \kappa_{e\pm}^2}} |F_e^+, m_e\rangle + \frac{\kappa_{e\pm}}{\sqrt{1 + \kappa_{e\pm}^2}} |F_e^-, m_e\rangle$$

$$\kappa_{g\pm} = \frac{2(2I+1)(\Lambda_g^\pm - \zeta) + 2\mu_B f_g m_g B}{\mu_B g_g B \sqrt{(2I+1)^2 - 4m_g^2}}$$

and

$$\kappa_{e\pm} = \frac{2(2I+1)(\Lambda_e^\pm - \zeta) + 2\mu_B f_e m_e B}{\mu_B g_e B \sqrt{(2I+1)^2 - 4m_e^2}}$$

Analytical treatment

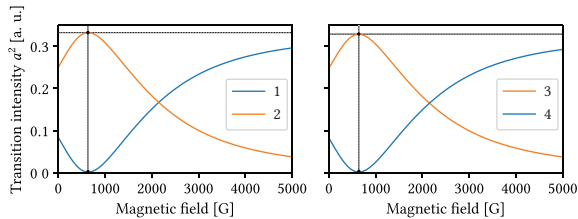


Figure: Possible π transition intensities for a general system of two ground magnetic sublevels and two excited magnetic sublevels with $I = 3/2$ and $m = -1$.

Analytical treatment

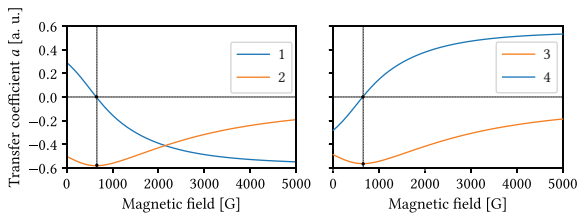


Figure: Possible π transfer coefficients for a general system of two ground magnetic sublevels and two excited magnetic sublevels with $I = 3/2$ and $m = -1$.

Analytical treatment

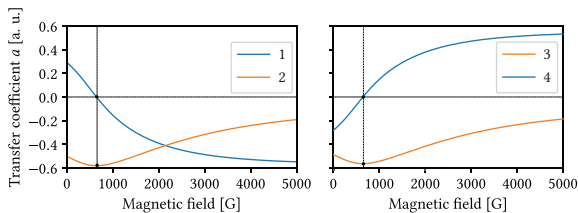


Figure: Possible π transfer coefficients for a general system of two ground magnetic sublevels and two excited magnetic sublevels with $I = 3/2$ and $m = -1$.

Possible cases

- 1 : $|F_g^-, m\rangle \rightarrow |F_e^-, m\rangle$
 - 2 : $|F_g^+, m\rangle \rightarrow |F_e^-, m\rangle$
 - 3 : $|F_g^-, m\rangle \rightarrow |F_e^+, m\rangle$
 - 4 : $|F_g^+, m\rangle \rightarrow |F_e^+, m\rangle$

Analytical treatment

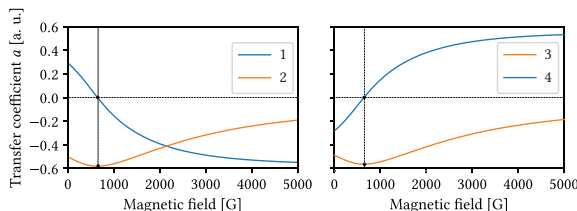


Figure: Possible π transfer coefficients for a general system of two ground magnetic sublevels and two excited magnetic sublevels with $I = 3/2$ and $m = -1$.

Possible cases

- 1 : $|F_g^-, m\rangle \rightarrow |F_e^-, m\rangle$
- 2 : $|F_g^+, m\rangle \rightarrow |F_e^-, m\rangle$
- 3 : $|F_g^-, m\rangle \rightarrow |F_e^+, m\rangle$
- 4 : $|F_g^+, m\rangle \rightarrow |F_e^+, m\rangle$

Cancellation and maximization

$$B = -\frac{4m\zeta\epsilon}{\mu_B(2I+1)(g_g\epsilon + g_e\zeta)}$$

Cancellation (resp. maximization) occurs for $\Delta F = 0$ (resp. $\Delta F = \pm 1$).

Analytical results

Isotope	Index	<i>F</i>	<i>m</i>	<i>B</i> [G]	<i>B</i> * [G]
²³ Na	1	1	-1	153.2007(86)	153.2007024(11)
	2	2			
³⁹ K	3	1		44.991(10)	44.9915(37)
	4	2			
⁴¹ K	5	1		24.042(95)	24.0418(30)
	6	2			

Isotope	Index	F	m	B [G]	B* [G]
^{40}K	1	$9/2^-$	7/2	190.20(33)	190.204(13)
	2	$7/2^-$			
	3	$9/2^-$	5/2	135.85(24)	135.8602(98)
	4	$7/2^-$			
	5	$9/2^-$	3/2	81.5(15)	81.5161(59)
	6	$7/2^-$			
	7	$9/2^-$	1/2	27.171(48)	27.1720(19)
	8	$7/2^-$			

Isotope	Index	F	m	B [G]	B* [G]
^{133}Cs	1	3	-3	1359.237(26)	1359.2372467(92)
	2	4			
	3	3	-2	906.158(17)	906.1581644(61)
	4	4			
	5	3	-1	453.0790(84)	453.0790822(31)
	6	4			

Isotope	Excited state	Cancelled			Magnetic field		Maximised		
		Index	F	m	B [G]	B* [G]	Index	ΔF	m
⁸⁵ Rb	$5^2P_{1/2}$	1	2	-2	380.73(13)	380.7362466(29)	5	-1	-2
		2	3				6	+1	
		3	2	-1	190.368(66)	190.3681233(15)	7	-1	-1
		4	3				8	+1	
	$6^2P_{1/2}$	1	2	-2	150.31(76)	150.31738954(20)	5	-1	-2
		2	3				6	+1	
		3	2	-1	75.15(38)	75.15869477(10)	7	-1	-1
		4	3				8	+1	
⁸⁷ Rb	$5^2P_{1/2}$	1	1	-1	642.590(76)	642.5904743(48)	3	-1	-1
		2	2				4	+1	
	$6^2P_{1/2}$	1	1	-1	254.39(57)	254.398160387(80)	3	-1	
		2	2				4	+1	-1

Experimental feasibility

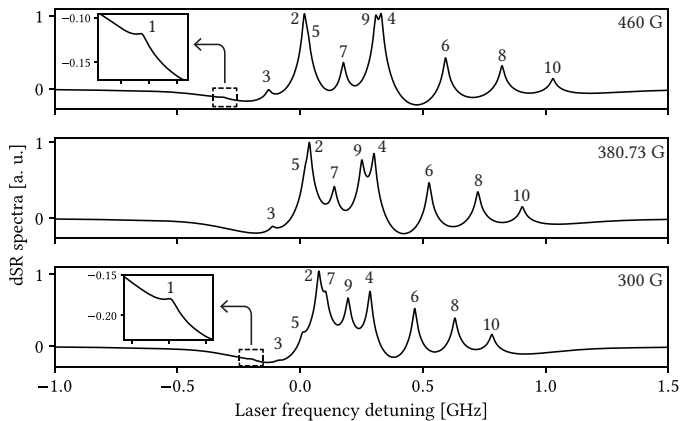


Figure: dSR spectra of ^{85}Rb D_1 line $F = 2 \rightarrow F' = 2, 3$ π transitions for different magnetic field values. The parameters used for the simulation are $L = \lambda/2$, $P_L = 1 \mu\text{W}$, $T = 130^\circ\text{C}$. The dSR amplitudes are normalized to that of the second spectrum.

Introduction

Nanometric thin cell spectroscopy

Alkali vapors in a magnetic field

Transition cancellations

Magnetometry with thin cells

- Experimental results: magnetometry with a nanocell
 - Experimental results: magnetometry with a microcell

Conclusion

Experimental setup

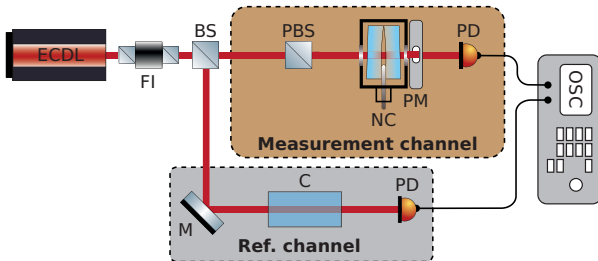


Figure: Experimental setup. ECDL: extended-cavity diode laser ($\lambda = 770$ nm), FI: Faraday isolator, NC: nanocell filled with K atoms. The thickness L of the vapor column can be adjusted in the range $120 - 390$ nm. BS: beam splitter, PBS: polarizing beam splitter, C: auxiliary cm-long cell filled with K used to form a reference SA spectrum, PM: permanent magnet, M: mirror. **B** is oriented along the laser propagation direction, PD: photo-detectors, OSC: oscilloscope.

M. Auzinsh, A. Sargsyan, A. Tonoyan, C. Leroy, R. Momier, D. Sarkisyan, and A. Papoyan. *Wide range linear magnetometer based on a sub-micro sized K vapor cell*. *Appl. Opt.* **61** (19) (2022), p. 5749.

Potassium in the HPB regime

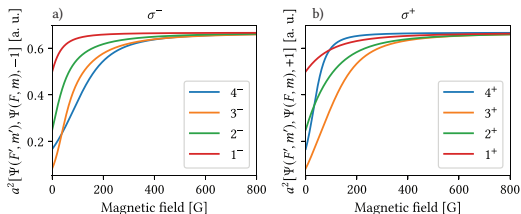


Figure: Magnetic field dependence of the strongest (in the HPB regime) Zeeman transitions of the D_1 line of ^{39}K . a) σ^- transitions. b) σ^+ transitions.

Potassium in the HPB regime

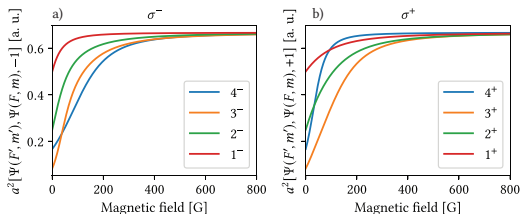


Figure: Magnetic field dependence of the strongest (in the HPB regime) Zeeman transitions of the D_1 line of ^{39}K . a) σ^- transitions. b) σ^+ transitions.

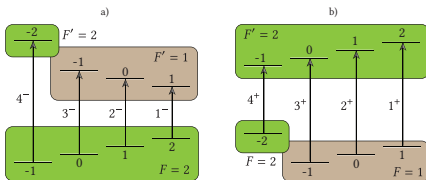


Figure: Transition diagram. a) σ^- transitions. b) σ^+ transitions.

Results - Spectra

With this simple setup, we track the evolution of the Zeeman transitions while the magnet is brought farther from the cell.

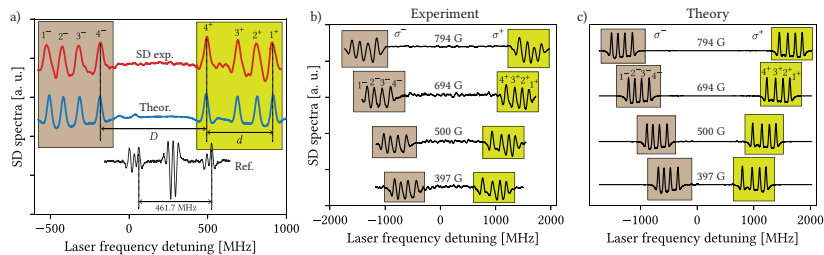


Figure: a) ^{39}K D_1 line spectra recorded for $L = 385$ nm. b) Experimental SD spectra for σ polarized radiation recorded for $B = 397, 500, 654$ and 794 G. c) Theoretical SD spectra for the same values of B_z .

Results - Magnetic field measurement

Let us compare D and D/d with the theory:

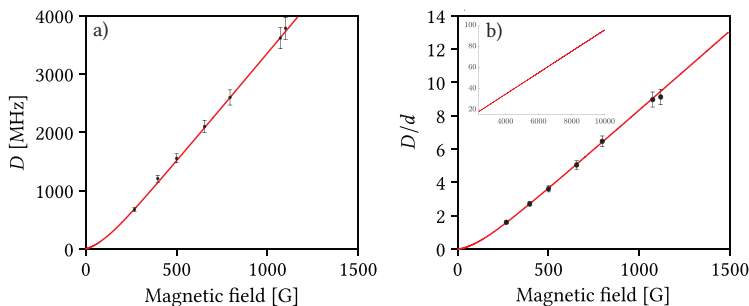


Figure: a) Frequency difference D between transitions 4^+ and 4^- as a function of the magnetic field. Solid line: theory. Dots with error bars: experimental measurements. b) D/d as a function of the magnetic field. Solid line: theory. Dots with error bars: experimental measurements. In both cases, the inaccuracy is around 5%. The inset shows the theoretical ratio D/d with respect to the magnetic field up to $B = 10$ kG.

Results - Gradient measurement

The spectral resolution allows to measure fields with a gradient of at least $3.5 \text{ G}/\mu\text{m}$.

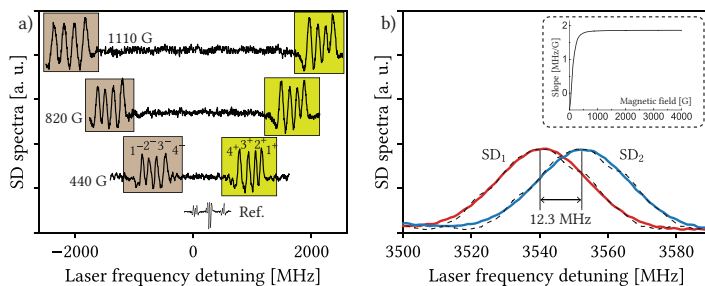


Figure: ^{39}K D_1 line spectra recorded for $L = 120 \pm 5$ nm. a) SD absorption spectra for B_z increasing from 440 to 1110 G. Lower curve: SD of a saturated absorption spectrum for reference. σ^- and σ^+ are shown in the brown and green regions respectively. b) The red curve has been calculated for $B_1 = 2000$ G and the blue curve for $B_2 = 2007$ G. Black curves depict experimental SD absorption spectra for B_1 and B_2 .

Experimental setup

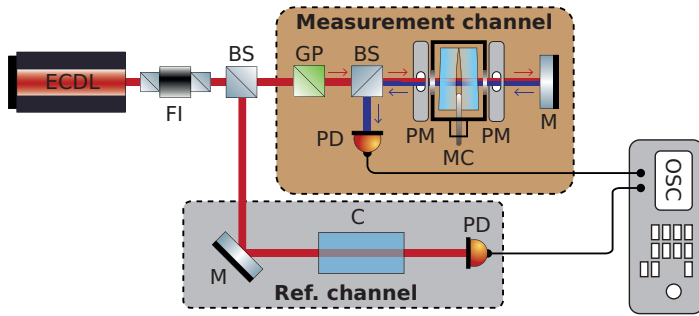


Figure: Sketch of the SA experimental setup using a MC. ECDL: Extended Cavity Diode-Laser, $\lambda = 770$ nm. FI: Faraday Isolator, BS: beam splitter, GP: Glan polarizer, MC: Micrometric-Thin ^{39}K Cell. C: cm-long cell used to form a SA reference spectrum at $B = 0$. PM: permanent magnet, PD: photodetector, M: mirror, OSC: oscilloscope.

Experimental setup

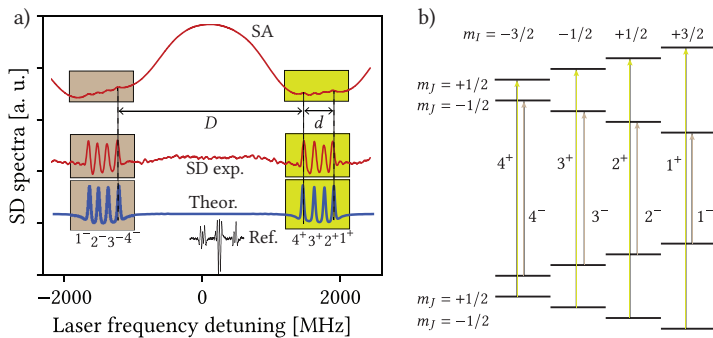


Figure: a) Upper curve: experimental SA spectrum of the D_1 line of ^{39}K obtained using a MC and linearly polarized laser radiation when a longitudinal magnetic field $B = 822$ G is applied. Middle curve (SD exp.): SD of the SA spectrum (inverted for convenience). The σ^- and σ^+ transitions are represented in the brown and green boxes, respectively. Blue curve (Theor.): SD of a theoretical absorption spectrum. Bottom black curve: SD of a reference ($B = 0$) SA spectrum obtained with a 1.5 cm-long ^{39}K cell. b) Diagram depicting the 8 σ^\pm transitions present in the HPB regime in the uncoupled basis $|m_I, m_J\rangle$. The transitions obey the selection rules $\Delta J = 0$, $\Delta m_I = 0$ and $\Delta m_J = \pm 1$ for σ^\pm radiation. σ^+ and σ^- transitions are respectively shown in green and brown.

Experimental setup

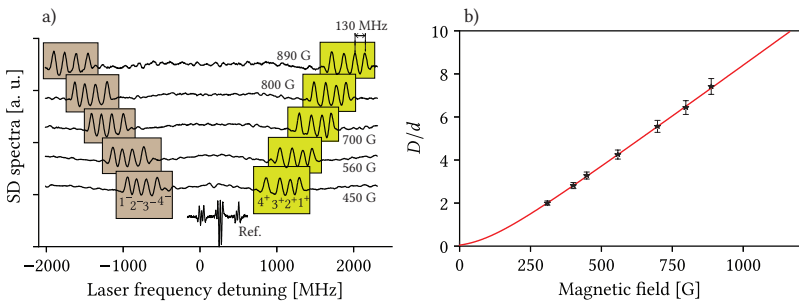


Figure: SD of experimental SA spectra obtained using a MC filled with ^{39}K probed with linearly polarized laser radiation. The longitudinal magnetic field B_z is gradually increased from 450 to 890 G. The frequency distance between any two neighboring transitions is ~ 130 MHz. Bottom black curve: SA of a reference ($B = 0$) SA spectrum obtained with a 1.5 cm-long ^{39}K cell.

Introduction

Nanometric thin cell spectroscopy

Alkali vapors in a magnetic field

Transition cancellations

Magnetometry with thin cells

EIT resonances using “forbidden” transitions

- Theoretical considerations
- Experimental results

Conclusion

Brief recap of the theoretical model

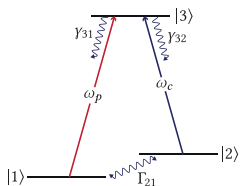


Figure: Scheme of the three-level A-system used in the calculations. The total decay rate Γ_{33} of state $|3\rangle$ is $1/2(\gamma_{31} + \gamma_{32})$.

B. W. Shore. *The Theory of Coherent Atomic Excitation, Simple Atoms and Fields.* (1990).

Y. Pashayan-Leroy, C. Leroy, A. Sargsyan, A. Papoyan, and D. Sarkisyan. Electromagnetically induced transparency: the thickness of the vapor column is of the order of a light wavelength. *JOSA B* 24 (8) (2007), pp. 1829–1838.

Brief recap of the theoretical model

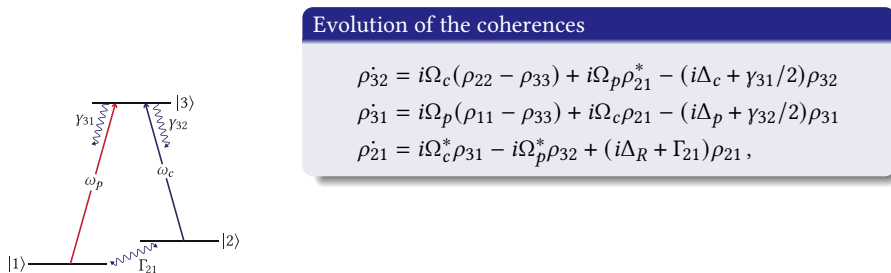


Figure: Scheme of the three-level Λ -system used in the calculations. The total decay rate Γ_{33} of state $|3\rangle$ is $1/2(\gamma_{31} + \gamma_{32})$.

B. W. Shore. *The Theory of Coherent Atomic Excitation, Simple Atoms and Fields.* (1990).

Y. Pashayan-Leroy, C. Leroy, A. Sargsyan, A. Papoyan, and D. Sarkisyan. Electromagnetically induced transparency: the thickness of the vapor column is of the order of a light wavelength. *JOSA B* 24 (8) (2007), pp. 1829–1838.

Brief recap of the theoretical model

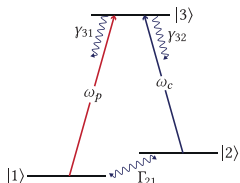


Figure: Scheme of the three-level A-system used in the calculations. The total decay rate Γ_{33} of state $|3\rangle$ is $1/2(\gamma_{31} + \gamma_{32})$.

Evolution of the coherences

$$\begin{aligned}\dot{\rho}_{32} &= i\Omega_c(\rho_{22} - \rho_{33}) + i\Omega_p\rho_{21}^* - (i\Delta_c + \gamma_{31}/2)\rho_{32} \\ \dot{\rho}_{31} &= i\Omega_p(\rho_{11} - \rho_{33}) + i\Omega_c\rho_{21} - (i\Delta_p + \gamma_{32}/2)\rho_{31} \\ \dot{\rho}_{21} &= i\Omega_c^*\rho_{31} - i\Omega_p^*\rho_{32} + (i\Delta_R + \Gamma_{21})\rho_{21},\end{aligned}$$

Absorption spectrum

$$\begin{aligned}\langle A \rangle &= \frac{-4\pi\omega_p N t_2^2 t_1}{cu\sqrt{u}} \frac{E_p}{|F|^2} \int_0^{+\infty} v_z M(v_z) dv_z \int_0^{L/v} dt \\ &\times \text{Im} \left\{ d_{31} \left[\rho_{31}^+ \left(t, \Delta_p^+, E_{p0}(v_z t) \right) \left(1 - r_1 e^{2ik_p v_z t} \right) \right. \right. \\ &\left. \left. + \rho_{31}^- \left(t, \Delta_p^-, E_{p0}(L - v_z t) \right) \left(1 - r_1 e^{2ik_p(L-v_z t)} \right) \right] \right\}\end{aligned}$$

B. W. Shore. *The Theory of Coherent Atomic Excitation, Simple Atoms and Fields.* (1990).

Y. Pashayan-Leroy, C. Leroy, A. Sargsyan, A. Papoyan, and D. Sarkisyan. *Electromagnetically induced transparency: the thickness of the vapor column is of the order of a light wavelength.* JOSA B 24 (8) (2007), pp. 1829–1838.

Forbidden transitions

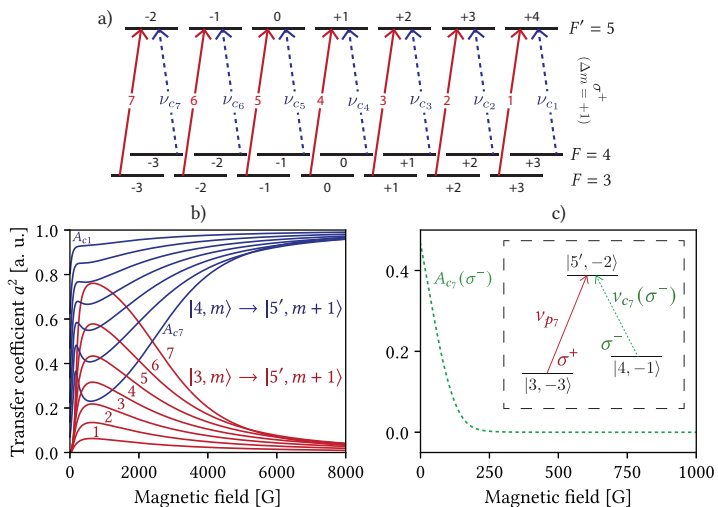


Figure: a) Scheme of Cs D_2 line σ^+ transitions between $F = 3, 4$ and $F' = 5$ and (b-c) magnetic field dependence of the Zeeman transition intensities of the D_2 line of Cs. b) $F = 3 \rightarrow F' = 5$ σ^+ MI transitions and $F = 4 \rightarrow F' = 5$ σ^+ transitions. c) Transition $|4, -1\rangle \rightarrow |5', -2\rangle (\sigma^-)$.

Experimental setup

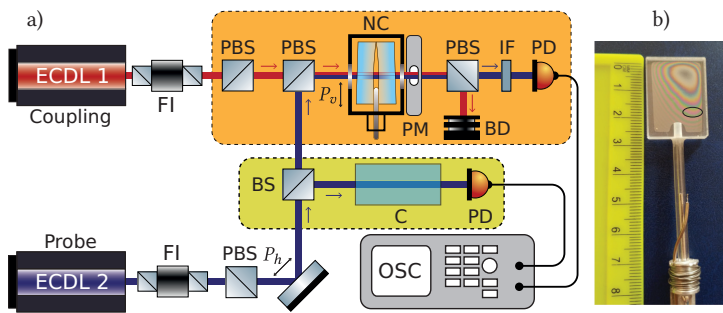


Figure: a) Scheme of the EIT experimental setup. ECDL: CW narrow-band external-cavity diode lasers with $\lambda = 852$ nm (resonant with Cs D_2 line). FI: Faraday insulators. PBS: polarizing beam splitters. BS: beam splitter. IF: interference filter. C: saturated absorption spectroscopy unit for frequency reference. NC: nanocell placed in oven. PM: permanent magnet. PD: photodiodes. OSC: 4-channel digital oscilloscope. P_h and P_v stand for horizontal and vertical polarizations. b) Picture of the nanocell. The oval corresponds to the region where $L \approx \lambda$.

A. Sargsyan, A. Tonoyan, R. Momier, C. Leroy, and D. Sarkisyan. *Formation of strongly shifted EIT resonances using “forbidden” transitions of Cesium*. J. Quant. Spectrosc. Radiat. Transf. 303 (2023), p. 108582.

Experimental results

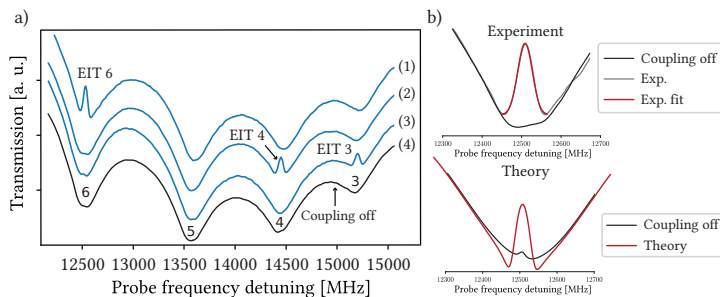


Figure: a) Probe transmission spectra of the Cs nanocell ($L = \lambda = 852$ nm). Lines 1 to 3 show three EIT resonances, labeled EIT 3, EIT 4 and EIT 6. The external longitudinal magnetic field is $B = 2880$ G. Line 4 is a probe transmission spectrum when the coupling is off. b) Zoom on EIT 6 fitted with a Gaussian profile (FWHM 35 MHz) and comparison with theoretical calculations. The intensity of the coupling radiation was 18 mW/cm 2 . Red: coupling on, black: coupling off. Small VSOP peaks are visible on each atomic transition formed by the probe radiation. Their typical linewidth is 40-50 MHz. Zero frequency corresponds to the transition frequency of Cs D_2 line.

A. Sargsyan, A. Tonoyan, R. Momier, C. Leroy, and D. Sarkisyan. *Formation of strongly shifted EIT resonances using “forbidden” transitions of Cesium*. J. Quant. Spectrosc. Radiat. Transf. 303 (2023), p. 108582.

Experimental results

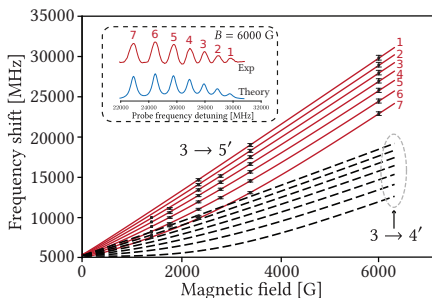


Figure: Red solid lines: frequency shift of transitions 1 to 7 as a function of the magnetic field. The black squares with error bars represent experimental measurements performed using absorption spectra. The uncertainties for the measurements were derived from the non-linearity of the laser scanning which was evaluated to be around 1% throughout the spectral range. Black dashed lines: frequency shift of $F_g = 3 \rightarrow F_e = 4$ transitions. For $B > 3$ kG, both groups are well separated in frequency. Inset: theoretical and experimental absorption spectra for $B = 6$ kG, the frequency shift reaches 30 GHz from the Cs D_2 line transition frequency.

A. Sargsyan, A. Tonoyan, R. Momier, C. Leroy, and D. Sarkisyan. *Formation of strongly shifted EIT resonances using “forbidden” transitions of Cesium*. J. Quant. Spectrosc. Radiat. Transf. **303** (2023), p. 108582.

Nanometric thin cell spectroscopy

Alkali vapors in a magnetic field

Transition cancellations

Magnetometry with thin cells

Conclusion

Conclusion and perspectives

What has been done

- Verify the NC model and compare it with experimental predictions
 - Study atom-surface interactions and observe retardation of the C_3 coefficient
 - Provide a complete description of all Zeeman transitions of Sodium D lines
 - Derived a theoretical framework for transition dipole moment cancellation
 - Used NCs and MCs to perform magnetometry with a good spatial resolution
 - Demonstrated the possibility of forming EIT resonances with forbidden transitions of Cesium

Conclusion and perspectives

What has been done

- Verify the NC model and compare it with experimental predictions
 - Study atom-surface interactions and observe retardation of the C_3 coefficient
 - Provide a complete description of all Zeeman transitions of Sodium D lines
 - Derived a theoretical framework for transition dipole moment cancellation
 - Used NCs and MCs to perform magnetometry with a good spatial resolution
 - Demonstrated the possibility of forming EIT resonances with forbidden transitions of Cesium

Conclusion and perspectives

What has been done

- Verify the NC model and compare it with experimental predictions
 - Study atom-surface interactions and observe retardation of the C_3 coefficient
 - **Provide a complete description of all Zeeman transitions of Sodium D lines**
 - Derived a theoretical framework for transition dipole moment cancellation
 - Used NCs and MCs to perform magnetometry with a good spatial resolution
 - Demonstrated the possibility of forming EIT resonances with forbidden transitions of Cesium

Conclusion and perspectives

What has been done

- Verify the NC model and compare it with experimental predictions
 - Study atom-surface interactions and observe retardation of the C_3 coefficient
 - Provide a complete description of all Zeeman transitions of Sodium D lines
 - **Derived a theoretical framework for transition dipole moment cancellation**
 - Used NCs and MCs to perform magnetometry with a good spatial resolution
 - Demonstrated the possibility of forming EIT resonances with forbidden transitions of Cesium

Conclusion and perspectives

What has been done

- Verify the NC model and compare it with experimental predictions
 - Study atom-surface interactions and observe retardation of the C_3 coefficient
 - Provide a complete description of all Zeeman transitions of Sodium D lines
 - Derived a theoretical framework for transition dipole moment cancellation
 - **Used NCs and MCs to perform magnetometry with a good spatial resolution**
 - Demonstrated the possibility of forming EIT resonances with forbidden transitions of Cesium

Conclusion and perspectives

What has been done

- Verify the NC model and compare it with experimental predictions
 - Study atom-surface interactions and observe retardation of the C_3 coefficient
 - Provide a complete description of all Zeeman transitions of Sodium D lines
 - Derived a theoretical framework for transition dipole moment cancellation
 - Used NCs and MCs to perform magnetometry with a good spatial resolution
 - **Demonstrated the possibility of forming EIT resonances with forbidden transitions of Cesium**

Conclusion and perspectives

What has been done

- Verify the NC model and compare it with experimental predictions
 - Study atom-surface interactions and observe retardation of the C_3 coefficient
 - Provide a complete description of all Zeeman transitions of Sodium D lines
 - Derived a theoretical framework for transition dipole moment cancellation
 - Used NCs and MCs to perform magnetometry with a good spatial resolution
 - Demonstrated the possibility of forming EIT resonances with forbidden transitions of Cesium

Conclusion and perspectives

What has been done

- Verify the NC model and compare it with experimental predictions
 - Study atom-surface interactions and observe retardation of the C_3 coefficient
 - Provide a complete description of all Zeeman transitions of Sodium D lines
 - Derived a theoretical framework for transition dipole moment cancellation
 - Used NCs and MCs to perform magnetometry with a good spatial resolution
 - Demonstrated the possibility of forming EIT resonances with forbidden transitions of Cesium

What can/needs to be done now

- Clean up the codes and release a Python package for spectra calculations in a magnetic field taking into account the geometry of the cell.
 - Release an atlas summarizing all transition cancellation values
 - Refine the magnetometry setup
 - A Python package similar to the one released by Downes for arbitrarily shaped systems with an arbitrary (but reasonable) number of levels and lasers is being written.

Conclusion and perspectives

What has been done

- Verify the NC model and compare it with experimental predictions
 - Study atom-surface interactions and observe retardation of the C_3 coefficient
 - Provide a complete description of all Zeeman transitions of Sodium D lines
 - Derived a theoretical framework for transition dipole moment cancellation
 - Used NCs and MCs to perform magnetometry with a good spatial resolution
 - Demonstrated the possibility of forming EIT resonances with forbidden transitions of Cesium

What can/needs to be done now

- Clean up the codes and release a Python package for spectra calculations in a magnetic field taking into account the geometry of the cell.
 - Release an atlas summarizing all transition cancellation values
 - Refine the magnetometry setup
 - A Python package similar to the one released by Downes for arbitrarily shaped systems with an arbitrary (but reasonable) number of levels and lasers is being written.

Conclusion and perspectives

What has been done

- Verify the NC model and compare it with experimental predictions
 - Study atom-surface interactions and observe retardation of the C_3 coefficient
 - Provide a complete description of all Zeeman transitions of Sodium D lines
 - Derived a theoretical framework for transition dipole moment cancellation
 - Used NCs and MCs to perform magnetometry with a good spatial resolution
 - Demonstrated the possibility of forming EIT resonances with forbidden transitions of Cesium

What can/needs to be done now

- Clean up the codes and release a Python package for spectra calculations in a magnetic field taking into account the geometry of the cell.
 - Release an atlas summarizing all transition cancellation values
 - Refine the magnetometry setup
 - A Python package similar to the one released by Downes for arbitrarily shaped systems with an arbitrary (but reasonable) number of levels and lasers is being written.

Conclusion and perspectives

What has been done

- Verify the NC model and compare it with experimental predictions
 - Study atom-surface interactions and observe retardation of the C_3 coefficient
 - Provide a complete description of all Zeeman transitions of Sodium D lines
 - Derived a theoretical framework for transition dipole moment cancellation
 - Used NCs and MCs to perform magnetometry with a good spatial resolution
 - Demonstrated the possibility of forming EIT resonances with forbidden transitions of Cesium

What can/needs to be done now

- Clean up the codes and release a Python package for spectra calculations in a magnetic field taking into account the geometry of the cell.
 - Release an atlas summarizing all transition cancellation values
 - Refine the magnetometry setup
 - A Python package similar to the one released by Downes for arbitrarily shaped systems with an arbitrary (but reasonable) number of levels and lasers is being written.

Outcome

- R. Momier, A. Aleksanyan, E. Gazazyan, A. Papoyan, and C. Leroy. *New standard magnetic field values determined by cancellations of ^{85}Rb and ^{87}Rb atomic vapors $5^2\text{S}_{1/2} \rightarrow 6^2\text{P}_{1/2,3/2}$ transitions*. *J. Quant. Spectrosc. Radiat. Transf.* **257** (2020), p. 107371
 - A. Aleksanyan, R. Momier, E. Gazazyan, A. Papoyan, and C. Leroy. *Transition cancellations of ^{87}Rb and ^{85}Rb atoms in a magnetic field*. *J. Opt. Soc. Am. B* **37** (11) (2020), 3504–3514
 - R. Momier, A. V. Papoyan, and C. Leroy. *Sub-Doppler spectra of sodium D lines in a wide range of magnetic field: Theoretical study*. *J. Quant. Spectrosc. Radiat. Transf.* **272** (2021), p. 107780
 - A. Sargsyan, R. Momier, A. Papoyan, and D. Sarkisyan. *Sub-Doppler Spectroscopy of Room-Temperature Cs Atomic Vapor in a 400-nm-Thick Nanocell*. *J. Exp. Theor. Phys.* **133** (4) (2021), pp. 404–410
 - A. Sargsyan, A. Tonoyan, R. Momier, C. Leroy, and D. Sarkisyan. *Dominant magnetically induced transitions in alkali metal atoms with nuclear spin 3/2*. *J. Opt. Soc. Am. B* **39** (4) (2022), p. 973
 - M. Auzinsh, A. Sargsyan, A. Tonoyan, C. Leroy, R. Momier, D. Sarkisyan, and A. Papoyan. *Wide range linear magnetometer based on a sub-microsized K vapor cell*. *Appl. Opt.* **61** (19) (2022), p. 5749
 - A. Sargsyan, R. Momier, C. Leroy, and D. Sarkisyan. *Saturated absorption technique used in potassium microcells for magnetic field sensing*. *Laser Phys.* **32** (10) (2022), p. 105701
 - A. Aleksanyan, R. Momier, E. Gazazyan, A. Papoyan, and C. Leroy. *Cancellation of D_1 line transitions of alkali-metal atoms by magnetic-field values*. *Phys. Rev. A* **105** (4) (2022), p. 042810
 - A. Sargsyan, A. Tonoyan, R. Momier, C. Leroy, and D. Sarkisyan. *Formation of strongly shifted EIT resonances using “forbidden” transitions of Cesium*. *J. Quant. Spectrosc. Radiat. Transf.* **303** (2023), p. 108582
 - A. Sargsyan, R. Momier, C. Leroy, and D. Sarkisyan. *Competing van der Waals and dipole-dipole interactions in optical nanocells at thicknesses below 100 nm*. *Phys. Lett. A* **483** (2023), p. 129069
 - A. Tonoyan, A. Sargsyan, R. Momier, C. Leroy, and D. Sarkisyan. *Formation of Narrow Atomic Lines of Rb in the UV Region Using a Magnetic Field*. *Opt. Mem. Neural Networks* **32** (S3) (2023), S343–S348
 - R. Momier, A. Sargsyan, A. Tonoyan, C. Leroy, and D. Sarkisyan. *Micrometric-Thin Cell Filled with Rb Vapor for High-Resolution Atomic Spectroscopy*. *Opt. Mem. Neural Networks* **32** (3) (2023), S349–S355

Thank you for your attention !

References

- [1] G. Dutier, S. Saltiel, D. Bloch, and M. Ducloy. *Revisiting optical spectroscopy in a thin vapor cell: mixing of reflection and transmission as a Fabry–Perot microcavity effect*. *J. Opt. Soc. Am. B* **20** (5) (2003), 793–800. 11, 12, 13, 14
 - [2] M. Auzinsh, D. Budker, and S. M. Rochester. *Optically Polarized Atoms : Understanding Light-Atom Interactions*. (2010). 17, 18, 19, 20
 - [3] P. Tremblay, A. Michaud, M. Levesque, S. Thériault, M. Breton, J. Beaubien, and N. Cyr. *Absorption profiles of alkali-metal D lines in the presence of a static magnetic field*. *Phys. Rev. A* **42** (1990), 2766–2773. 25, 26, 27, 30, 31, 32, 33
 - [4] E. De Clercq, M. De Labachellerie, G. Avila, P. Cerez, and M. Tetu. *Laser diode optically pumped caesium beam*. *J. de Physique* **45** (2) (1984), pp. 239–247. 30, 31, 32, 33
 - [5] M. Auzinsh, A. Sargsyan, A. Tonoyan, C. Leroy, R. Momier, D. Sarkisyan, and A. Papoyan. *Wide range linear magnetometer based on a sub-microsized K vapor cell*. *Appl. Opt.* **61** (19) (2022), p. 5749. 62, 65, 66, 91
 - [6] B. W. Shore. *The Theory of Coherent Atomic Excitation, Simple Atoms and Fields*. (1990). 72, 73, 74
 - [7] Y. Pashayan-Leroy, C. Leroy, A. Sargsyan, A. Papoyan, and D. Sarkisyan. *Electromagnetically induced transparency: the thickness of the vapor column is of the order of a light wavelength*. *JOSA B* **24** (8) (2007), pp. 1829–1838. 72, 73, 74
 - [8] A. Sargsyan, A. Tonoyan, R. Momier, C. Leroy, and D. Sarkisyan. *Formation of*

Cancellation calculation equation

$$\frac{2 \sqrt{m}}{\sqrt{3} (1 + 2 \text{Inuc}) \sqrt{1 + \frac{4 (-\zeta + \frac{B(gI - 2gT) Inuc) m \mu}{1 + 2 \text{Inuc}} + \frac{1}{2} (\zeta - 2B gT m \mu) + \frac{1}{2} \left(\frac{4B(gI - gS) m^2 \mu}{1 + 2 \text{Inuc}} + \frac{B^2 (gI - gS)^2 \mu^2}{(1 + 2 \text{Inuc})^2} \right)^2)} + \sqrt{1 + \frac{36 (-B(4gI - gS - 6gT) Inuc) m \mu}{3 (1 + 2 \text{Inuc})} - \zeta + \frac{1}{2} (-2B gT m \mu + \zeta) + \frac{1}{2} \sqrt{\zeta^2 + \frac{4B(gI - gS) m^2 \mu}{1 + 2 \text{Inuc}} + B^2 (gI - gS)^2 \mu^2}})^2 + \\
 \frac{2 \left(-\zeta + \frac{B(gI - 2gT) Inuc) m \mu}{1 + 2 \text{Inuc}} + \frac{1}{2} (\zeta - 2B gT m \mu) + \frac{1}{2} \sqrt{\zeta^2 + \frac{4B(gI - gS) m^2 \mu}{1 + 2 \text{Inuc}} + B^2 (gI - gS)^2 \mu^2} \right)}{\sqrt{3} B (gI - gS) \mu \sqrt{1 + \frac{4 (-\zeta + \frac{B(gI - 2gT) Inuc) m \mu}{1 + 2 \text{Inuc}} + \frac{1}{2} (\zeta - 2B gT m \mu) + \frac{1}{2} \left(\frac{4B(gI - gS) m^2 \mu}{1 + 2 \text{Inuc}} + \frac{B^2 (gI - gS)^2 \mu^2}{(1 + 2 \text{Inuc})^2} \right)^2)} + \sqrt{1 + \frac{36 (-B(4gI - gS - 6gT) Inuc) m \mu}{3 (1 + 2 \text{Inuc})} - \zeta + \frac{1}{2} (-2B gT m \mu + \zeta) + \frac{1}{2} \sqrt{\frac{4}{9} B^2 (3gI - 4gL + gS)^2 \mu^2 + \frac{4B(3gI - 4gL + gS) m \mu \zeta}{3 (1 + 2 \text{Inuc})} + \zeta^2}})^2 + \\
 2 \sqrt{3} \left(\frac{B(4gI - gS - 6gT) Inuc) m \mu}{3 (1 + 2 \text{Inuc})} - \zeta + \frac{1}{2} (-2B gT m \mu + \zeta) + \frac{1}{2} \sqrt{\frac{4}{9} B^2 (3gI - 4gL + gS)^2 \mu^2 + \frac{4B(3gI - 4gL + gS) m \mu \zeta}{3 (1 + 2 \text{Inuc})} + \zeta^2} \right) + \\
 B (3gI - 4gL + gS) \mu \sqrt{1 + \frac{4 (-\zeta + \frac{B(gI - 2gT) Inuc) m \mu}{1 + 2 \text{Inuc}} + \frac{1}{2} (\zeta - 2B gT m \mu) + \frac{1}{2} \left(\frac{4B(gI - gS) m^2 \mu}{1 + 2 \text{Inuc}} + \frac{B^2 (gI - gS)^2 \mu^2}{(1 + 2 \text{Inuc})^2} \right)^2)} + \sqrt{1 + \frac{36 (-B(4gI - gS - 6gT) Inuc) m \mu}{3 (1 + 2 \text{Inuc})} - \zeta + \frac{1}{2} (-2B gT m \mu + \zeta) + \frac{1}{2} \sqrt{\frac{4}{9} B^2 (3gI - 4gL + gS)^2 \mu^2 + \frac{4B(3gI - 4gL + gS) m \mu \zeta}{3 (1 + 2 \text{Inuc})} + \zeta^2}})^2 + \\
 8 \sqrt{3} m \left(-\zeta + \frac{B(gI - 2gT) Inuc) m \mu}{1 + 2 \text{Inuc}} + \frac{1}{2} (\zeta - 2B gT m \mu) + \frac{1}{2} \sqrt{\zeta^2 + \frac{4B(gI - gS) m \zeta \mu}{1 + 2 \text{Inuc}} + B^2 (gI - gS)^2 \mu^2} \right) \\
 \left(\frac{B(4gI - gS + 6gT) Inuc) m \mu}{3 (1 + 2 \text{Inuc})} - \zeta + \frac{1}{2} (-2B gT m \mu + \zeta) + \frac{1}{2} \sqrt{\frac{1}{9} B^2 (3gI - 4gL + gS)^2 \mu^2 + \frac{4B(3gI - 4gL + gS) m \mu \zeta}{3 (1 + 2 \text{Inuc})} + \zeta^2} \right) / \\
 B^2 (gI - gS) (3gI - 4gL + gS) (1 + 2 \text{Inuc}) \left(1 - \frac{4m^2}{(1 + 2 \text{Inuc})^2} \right) \mu^2 \sqrt{1 + \frac{4 \left(-\zeta + \frac{B(gI - 2gT) Inuc) m \mu}{1 + 2 \text{Inuc}} + \frac{1}{2} (\zeta - 2B gT m \mu) + \frac{1}{2} \sqrt{\zeta^2 + \frac{4B(gI - gS) m^2 \mu}{1 + 2 \text{Inuc}} + B^2 (gI - gS)^2 \mu^2} \right)^2}{B^2 (gI - gS)^2 \left(1 - \frac{4m^2}{(1 + 2 \text{Inuc})^2} \right) \mu^2} + \\
 1 + \frac{36 \left(\frac{B(4gI - gS - 6gT) Inuc) m \mu}{3 (1 + 2 \text{Inuc})} - \zeta + \frac{1}{2} (-2B gT m \mu + \zeta) + \frac{1}{2} \sqrt{\frac{1}{9} B^2 (3gI - 4gL + gS)^2 \mu^2 + \frac{4B(3gI - 4gL + gS) m \mu \zeta}{3 (1 + 2 \text{Inuc})} + \zeta^2} \right)^2}{B^2 (3gI - 4gL + gS)^2 \left(1 - \frac{4m^2}{(1 + 2 \text{Inuc})^2} \right) \mu^2} \right)$$